Pulsed-CPT Cs-Ne microcell atomic clock with frequency stability below 2×10^{-12} at 10^5 s

CLÉMENT CARLÉ,[1] MOUSTAFA ABDEL HAFIZ,[1] SHERVIN KESHAVARZI,[1] RÉMY VICARINI,[1] NICOLAS PASSILLY,[1] AND RODOLPHE BOUDOT[1,*]

[1] *FEMTO-ST, CNRS, UFC, ENSMM, 26, rue de l'Epitaphe, 25030 Besançon, France*
[*] *rodolphe.boudot@femto-st.fr*

Abstract: We report on the mid-term stability progress of a table-top coherent population trapping (CPT) microcell atomic clock, previously limited by light-shift effects and variations of the cell inner atmosphere. The light-shift contribution is now mitigated through the use of a pulsed symmetric auto-balanced Ramsey (SABR) interrogation technique, combined with setup temperature, laser power and microwave power stabilization. In addition, Ne buffer gas pressure variations in the cell are now greatly reduced through the use of a micro-fabricated cell built with low permeation alumino-silicate glass (ASG) windows. Combining these approaches, the clock Allan deviation is measured to be 1.4×10^{-12} at 10^5 s. This stability level at 1 day is competitive with best current microwave microcell-based atomic clocks.

1. Introduction

Microwave chip-scale atomic clocks (CSACs) [1–6] based on coherent population trapping (CPT) [7] have met a significant success by offering a typical fractional frequency stability of a few 10^{-11} at 1 day integration time, in a low size, weight and power (SWaP) budget. These clocks are now deployed in navigation and positioning systems, secure communications, underwater sensor networks and unmanned vehicles. However, mid- and long-term instabilities remain and are likely to be resulting from light-shift effects and/or cell inner atmosphere evolution.

In a CPT CSAC, light-shifts are induced by variations of the laser power, laser frequency and microwave power and result in variations of the clock frequency. Various techniques have been demonstrated in continuous-regime (CW) CPT clocks to mitigate them such as the active stabilization on a specific microwave power set-point [8–11], the adjustment of the cell temperature [12], the compensation of the laser frequency detuning [11], the use of servo loops to mitigate variations of the laser block [6, 11, 13, 14], or the implementation of laser power modulation-based sequences [15, 16].

An alternative approach for light-shift mitigation consists in using pulsed Ramsey-based interrogation protocols. Their benefit for the improvement of mid- and long-term stability of vapor cell clocks, a specification of key importance for most of the applications, has been demonstrated in high-performance double-resonance Rb cell clocks with the pulsed-optically pumped (POP) method [17] or CPT clocks using symmetric auto-balanced Ramsey spectroscopy (SABR) [18]. These pulsed cell clocks have demonstrated long-term stability levels never achieved by their continuous-regime (CW) version. More recently, these interrogation methods were adopted with success in CPT [19, 20] and double-resonance microcell-based clocks [21].

Instabilities of the clock frequency can also be induced by any evolution of the cell inner atmosphere through the buffer-gas induced temperature and pressure shift of the atomic transition [22]. Buffer gas permeation through the cell glass windows has been identified as a limitation process [23], especially when light buffer gas, as helium or neon, are used. Reduction of helium permeation for ultra-high vacuum (UHV)-cell-based applications has been achieved by employing alumino-silicate glass (ASG) for the cell windows [24, 25]. However, to our knowledge, no data has been reported demonstrating the benefits of ASG as an efficient permeation barrier for microcells with other buffer gases.

In a previous study [20], we have undertaken the implementation of a CPT-based microcell atomic clock using symmetric auto-balanced Ramsey (SABR) spectroscopy for light-shift mitigation. Despite a reduction of the clock frequency sensitivity to light-field parameters by a factor higher than 100 in comparison with the standard continuous-wave (CW) regime, the clock stability remained limited for integration times higher than 1000 s by another mechanism, which we attributed to Ne permeation through the cell borosilicate glass (BSG) windows.

In this paper, we report on the stability performance progress of this pulsed CPT-based microcell atomic clock. The latter is not fully-integrated and uses an external acousto-optic modulator (AOM) for generation of the pulsed optical sequence. The clock, based now on a Cs-Ne microfabricated cell built with lower-permeation ASG windows, uses the SABR interrogation technique, in conjunction with active servos of the setup temperature, the microwave power, and the laser power. In this configuration, the clock Allan deviation reaches 1.4×10^{-12} at 10^5 s integration time. This stability result at 1 day is an order of magnitude better than reported in [20] and is competitive with those of best microwave clocks based on microcells [4, 14, 21].

2. Experimental set-up

Figure 1 describes the CPT clock experimental setup. This system was described in [20] and is briefly reminded here. The clock transition of Cs atoms, confined in a microfabricated vapor cell [26] filled with a pressure (~ 87 Torr) of Ne buffer gas, is probed by an optically-carried 9.192 GHz signal, obtained by direct current modulation at 4.596 GHz of a vertical-cavity surface-emitting laser (VCSEL) [27]. The laser is tuned on the Cs D_1 line (λ = 894.6 nm) and housed in a TO-46 package with integrated thermistance and Peltier element. The cell is temperature-stabilized at 75°C. A static magnetic field of 23.4 μT is applied to isolate the 0-0 clock transition. The cell is surrounded by a mu-metal magnetic shield to prevent magnetic perturbations from the environment.

An acousto-optic modulator (AOM), placed at the laser output, is used to chop the light and then produce the pulsed SABR interrogation sequence [20]. The latter is based on consecutive Ramsey sequences with optical pulses of duration T_b = 180 μs, followed either by a short dark time T_s of 100 μs or a long dark time T_L of 250 μs. The signal is detected at a time τ_d = 10 μs after the pulse trigger during a detection window of length τ_D = 10 μs. A beam splitting cube is used to collect a measurement of the laser power P_l at the cell input with a photodiode (PD1). The circularly-polarized light beam, with a diameter of about 0.5 mm, is transmitted through the vapor cell and detected by a second photodiode (PD2). The signal at the photodiode output is used in several servo loops for stabilization of the laser and the local oscillator frequencies, as well as for light-shift compensation. Optical sidebands that induce CPT resonance are connected to the Cs atom $6^2P_{1/2}$, F'= 4 excited state. The microwave synthesizer that delivers the 4.596 GHz signal is piloted by an active hydrogen maser used as a reference for frequency shifts and stability measurements.

The experimental setup is implemented onto a table-top optical breadboard. The latter is surrounded by a box with foam that provides passive temperature isolation. Two Schottky diodes were placed between the microwave synthesizer output and the VCSEL input bias-tee. The first one monitors the microwave power $P_{\mu W_i}$ of the incident 4.596 GHz signal at the synthesizer output while the second one measures through a microwave circulator the microwave power $P_{\mu W_r}$ reflected by the VCSEL. In this study, the impact of a microwave power servo was investigated. In this case, the microwave power $P_{\mu W_i}$, detected by one of the Schottky diodes, is converted into a voltage signal and hence compared to an ultra-stable voltage reference. An error signal, processed in a basic proportional-integral (PI) controller, is then used to correct the microwave

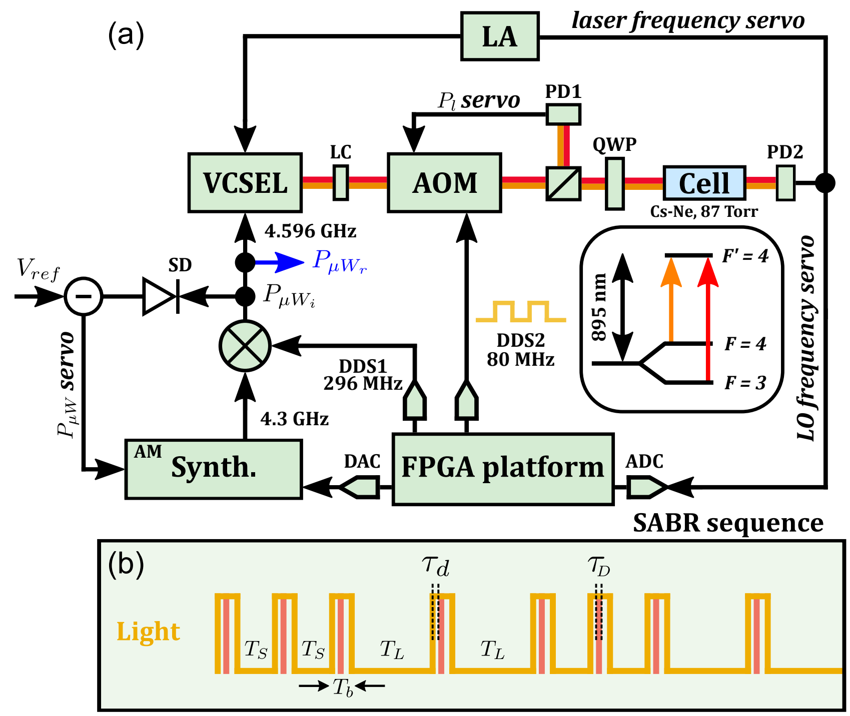

Fig. 1. (a): Schematic of the CPT clock experimental setup. A Cs vapor, diluted by a Ne buffer gas pressure in a microfabricated cell, interacts with optical CPT pulses generated with the help of a microwave-modulated VCSEL and an external AOM. AOM: acousto-optic moudulator, SD: Schottky diode, QWP: quarter-wave plate, LA: lock-in amplifier, ADC: analog-to-digital converter, DAC: digital-to-analog converter, Synth.: microwave synthesizer. The inset shows the energy levels of the Cs atom involved in the CPT interaction. (b): Light pattern produced in the SABR sequence [20].

power delivered by the microwave synthesizer. A comparable system was used to investigate the impact of laser power stabilization. In this case, the voltage signal at the output of the photodiode PD1 is compared to a voltage reference to provide a correction signal sent to the power of the RF signal that drives the AOM.

3. MEMS cell with ASG windows and setup temperature control

In our previous study [20], we suspected that Ne permeation through the cell glass windows could limit the clock frequency stability for integration times higher than 1000 s. To validate this assumption, we have developed a new wafer of Cs-Ne cells using low-permeation ASG windows [24]. Both BSG and ASG cells use the same dispenser technology and were laser-activated with comparable parameters. In this work, the Ne pressure at 0°C of BSG and ASG cells is estimated from [22] to be 88 ± 2 Torr and 87 ± 2 Torr, respectively. The Ne pressure in the cell induces for both cells a clock frequency shift of about 50 kHz. We remind here that the pressure shift coefficient for Cs clock transition in the presence of Ne gas is positive (686 ± 14 Hz /Torr) [22]. Thus, in our experiment, a leak of Ne gas leads to a progressive reduction of the clock frequency.

Figure 2 shows temporal traces of the clock frequency, recorded with the same experimental setup, but with two different Cs-Ne microcells, with windows made of BSG or ASG windows. The cell

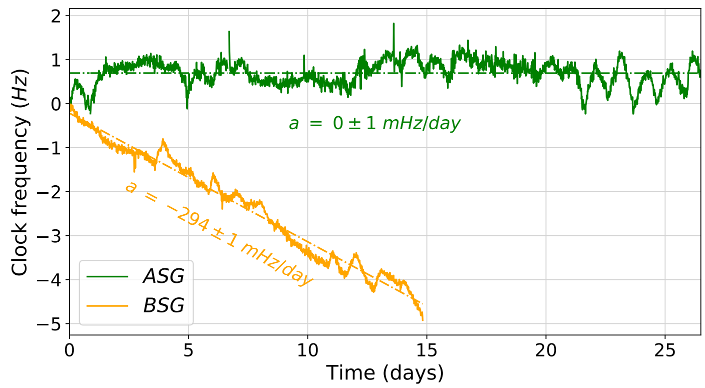

Fig. 2. Temporal trace of the clock frequency, using Cs-Ne microfabricated cells, having either BSG or ASG windows. For the ASG (BSG) cell, the 0 value on the y-axis corresponds to a central frequency of 9.192 682 333 (9.192 681 869) GHz. The initial clock frequency difference for the two cells is attributed to a slight difference of Ne pressure (~ 1 Torr).

with BSG windows leads to a negative clock frequency drift, assumed to be the signature of a Ne gas leak. The fitting of experimental data by a linear function yields a rate of −294 ± 1 mHz/day. This value is in good agreement with the clock frequency stability measured at 1 day when using a similar Cs-Ne cell heated at 70°C [20]. Fitting data by an exponential decay, we estimate the permeation rate for Neon through BSG to be about 3.3×10^{-22} $m^2.s^{-1}.Pa^{-1}$ at 75°C. Although this value is twice higher than the one reported in [28], it corresponds to the one extracted from a Cs-Ne clock frequency measurement performed at 81°C reported in [23]. With the cell having ASG windows, the clock is much more stable on the long-term. In this case, fitting of experimental data by a linear function gives a rate of 0 ± 1 mHz/day. These results strongly suggest that the use of ASG windows will mitigate the contribution of Ne gas permeation onto the clock long-term stability.

Despite the relevant improvement obtained with ASG, residual fluctuations of the clock frequency remain for shorter integration times, as it can be seen on Fig. 2. Looking at the

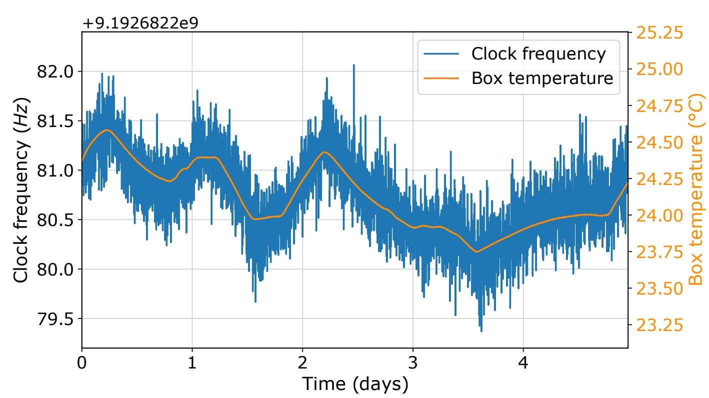

Fig. 3. Observed correlation between the clock frequency and the re-scaled setup box temperature. For information, the typical daily variations of the box temperature are 0.45°C. The maximum box temperature variations along the 5 days are 0.8°C.

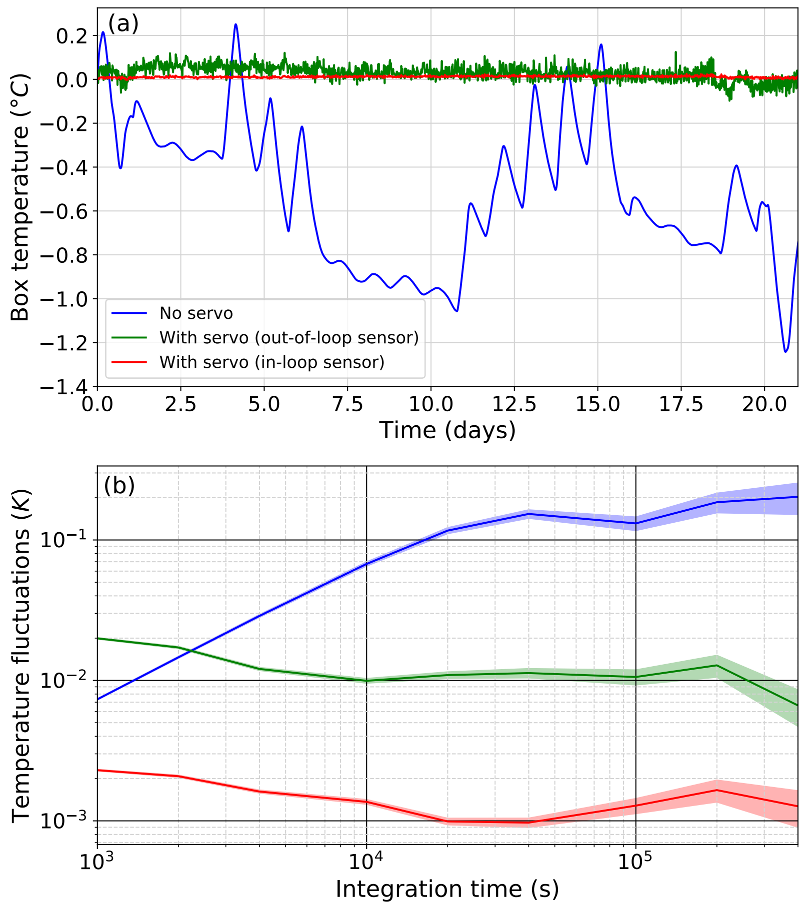

Fig. 4. (a) Temporal trace of the setup box temperature in normal and locked conditions. In the locked case, an in-loop and out-of-loop sensor are monitored. Offsets were applied to the temperatures for clarity. Temperatures at $t = 0$ are 26.2, 29.3 and 29°C for the "no servo", "with servo (out-of-loop)" and "with servo (in-loop)" cases, respectively. One point was kept every 1000 s. (b) Temperature fluctuations (K) of sensors, derived from data shown in (a), versus the integration time. The color code of Fig. 4(a) legend is kept. Colored zones indicate the size of error bars.

evolution of experimental parameters during the clock run, we found a clear correlation between the clock frequency and the setup box temperature variations. This behaviour is illustrated in Fig. 3 with another measurement data set of 5 days, where the box temperature was re-scaled, averaged for clarity and superimposed to the clock frequency data.

For better knowledge and control of the setup temperature, we have distributed over the setup breadboard 5 heating resistances and 7 thermistors. 6 sensors are used for monitoring while the seventh, placed between the quarter-wave plate and the CPT cell package, is used for the setup temperature control. The setup temperature in the box, measured at about 26°C (see Fig. 3 and caption) before implementation of the servo, was tuned at the level of about 29°C with the servo (see Fig. 4 and caption). This temperature remains much lower than the one of some key components of the setup such as the laser and the cell.

Figure 4(a) shows a temporal trace of the setup box temperature, measured for more than 20 days with an independent thermistor, with or without stabilization of the temperature. The temperature of the thermistor used by the temperature controller (in-loop sensor) is also reported for information. An averaging window of 1000 s is used to plot these data. We observe that temperature variations of the setup are drastically mitigated when the lock is activated. For complimentary information, Fig. 4(b) shows typical temperature fluctuations, extracted from data shown in Fig. 4(a), of the respective sensors, in free-running and locked cases, versus the integration time. Temperature variations of the out-of-loop sensor are reduced by one order of magnitude at 10^5 s in the locked case, yielding residual temperature fluctuations of about 0.01 K. The in-loop sensor shows temperature fluctuations around 1 mK at 10^5 s.

4. Clock frequency stability progress

This section reports on the evaluation progress of the clock fractional frequency stability. It aims to demonstrate how the clock stability was improved by progressively implementing additional servos of the setup box temperature, the microwave power and the laser power.

Figure 5 shows the clock Allan deviation recorded with the ASG cell, with or without stabilization of the setup box temperature. Microwave and power servos are not activated. The laser power P_l is 100 μW and the microwave power $P_{\mu W_i}$ is -0.49 dBm (0.89 mW). The blue curve of Fig. 5 shows results obtained without temperature stabilization of the setup box. In this case, the clock stability is limited at the level of about 10^{-11} at 10^5 s. When the setup temperature is stabilized (green curve), the clock Allan deviation is measured to be 1.5×10^{-10} at 1 s, 3.8×10^{-12} at 10^5 s and below 10^{-11} at 3×10^5 s. The clock stability at 1 day integration time is about one order of magnitude better than the one reported in [20], and is found in good agreement with the Allan deviation calculated from data shown in Fig. 3, where both the effect of the setup temperature and a residual linear drift (corresponding to permeation), would be subtracted from the raw data.

During clock operation, we have monitored some key experimental parameters in order to identify the new main contributions to the clock mid-term stability. In Fig. 5, the red curve depicts the contribution to the Allan deviation of the microwave power fluctuations. This contribution is derived from voltage fluctuations ΔV recorded at the output of the Schottky diode ($\Delta V/V = 7.2 \times 10^{-4}$ at 10^5 s) and includes fictitious input microwave power fluctuations induced by the temperature sensitivity of the Schottky diode power-to-voltage coefficient. With a measured dependence of the clock frequency to microwave power variations of 4.7×10^{-12} (in fractional value), this contribution reaches 3-4 $\times 10^{-12}$ at 10^5 s, a level comparable to the clock Allan

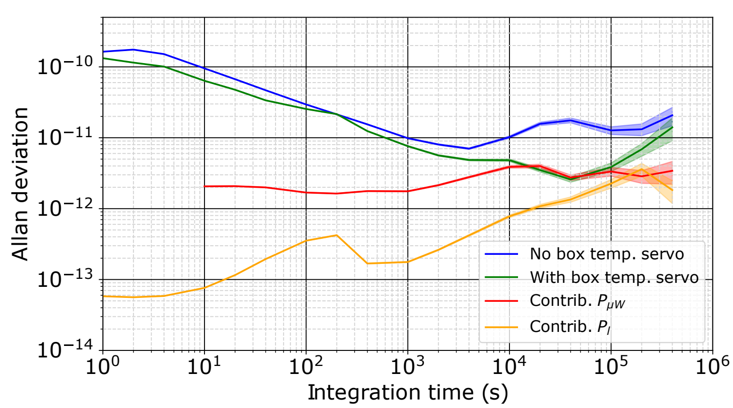

Fig. 5. Allan deviation of the clock frequency, with or without temperature stabilization of the setup breadboard. Contributions of the laser power and microwave power fluctuations to the clock Allan deviation are also shown. Colored zones indicate the size of error bars.

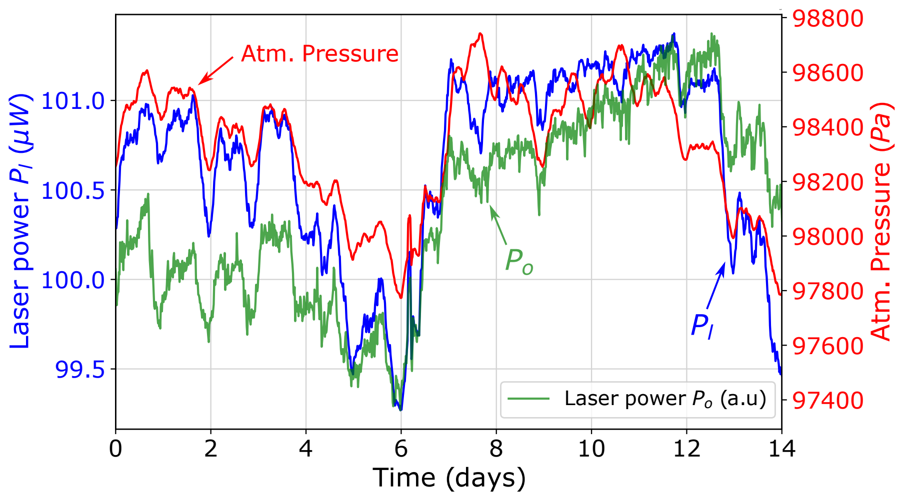

Fig. 6. Observed correlation between the atmospheric pressure, P_l the laser power at the cell input (PD1) and P_o the laser power at the cell output, measured in clock operation (PD2).

deviation result.

The second contribution to the clock stability, depicted by the orange curve in Fig. 5, is the contribution of laser power fluctuations. Here, laser power fluctuations at the cell input, obtained by measuring the laser power detected by the photodiode PD1 and adequate calibration, are multiplied by the sensitivity coefficient of the clock frequency versus laser power dependence curve ($6.5 \times 10^{-12}/\mu$W in fractional value). With fractional laser power fluctuations $\Delta P_l/P_l \simeq 3 \times 10^{-3}$ at 10^5 s ($\Delta P_l \simeq 0.3$ μW), we obtain that laser power fluctuations limit the clock stability at the level of about 2×10^{-12} at 10^5 s.

As shown in Fig. 6, we have noticed that the laser power P_l measured at the cell input (photodiode PD1), and consequently the laser power P_o at the cell output (PD2), were correlated with the atmospheric pressure measured in the lab. This can be explained by the fact that the VCSEL package used in this setup is not vacuum-sealed and then not immune to ambient pressure variations. Over a measurement of 6 days, we have also observed, without microwave power stabilization, that both microwave power signals, $P_{\mu W_i}$ and $P_{\mu W_r}$, showed periodically some spikes, also visible on the laboratory temperature data. This observation is consistent with the fact that some microwave components and detectors were initially out of the temperature-controlled setup box, experiencing ambient temperature fluctuations.

For further mitigation of light-shifts contributions, we have first envisioned to reduce the microwave power contribution shown in Fig. 5 (red curve). In this process, we studied the impact of the temperature dependence of the Schottky diode power-to-voltage coefficient. At fixed input microwave power, we measured that the voltage output of the Schottky diode could change at the level of -8×10^{-5} V/K. Given our experimental conditions, we calculated then that a variation of 1 K of the Schottky diode could induce, in closed-loop configuration of a microwave power servo, a clock frequency variation of 1.3×10^{-11}/K (in fractional value). With the Schottky diode out of the box and considering that 0.3 K temperature variation can be experienced within the experimental room, this sensitivity could have limited the clock stability at 10^5 s at the level of about 4×10^{-12}, comparable to the clock Allan deviation (green curve) of Fig. 5.

We placed first the Schottky diode into the temperature stabilized box, without microwave power servo. In this configuration, the contribution of the microwave power at 10^5 s, treated as in Fig.

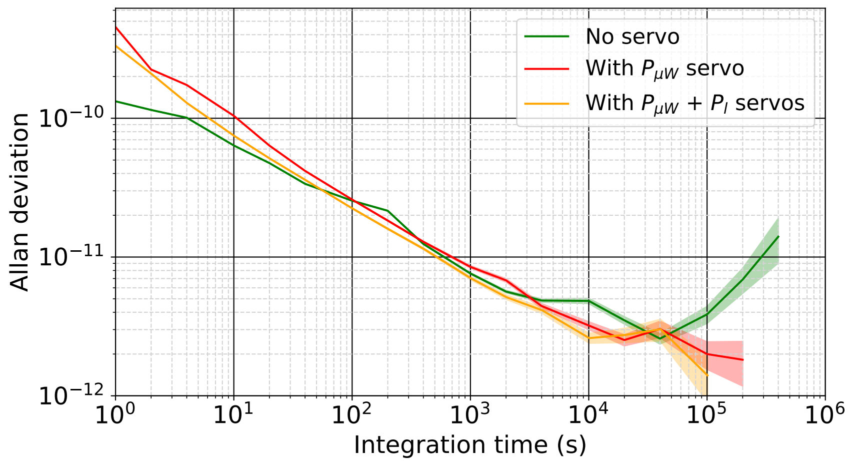

Fig. 7. Allan deviation of the clock frequency, with stabilization of the setup box temperature, in different configurations: no additional servos, with only microwave power servo, with microwave and laser power servo. Colored zones indicate the size of error bars.

5, was found to be comparable with the one measured in Fig. 5.

We have then implemented a microwave power servo, with the Schottky diode in the box. This test was performed with a comparable laser power $P_l \simeq 100\ \mu$W and a microwave power $P_{\mu W} \simeq 0.82$ mW. With this servo, microwave power fluctuations $\Delta P_{\mu W}/P_{\mu W}$, measured through the in-loop Schotky diode, were reduced at 1 day by almost an order of magnitude, reaching 9.7×10^{-5} ($\Delta P_{\mu W} \simeq 81$ nW at 1 day). With this number, the contribution of the microwave power variations to the clock stability would be rejected at the level of 3.8×10^{-13} at 10^5 s. With this servo, the clock frequency stability was improved, as shown in Fig. 7, at the level of 2×10^{-12} at 10^5 s and slightly below 2×10^{-12} at 2×10^5 s.

This level being comparable to the laser power contribution indicated in Fig. 5, we have performed a last stability test by adding the laser power servo. In this test, the laser power P_l was 75 μW while the microwave power was 0.73 mW. Using this servo, fractional laser power fluctuations $\Delta P_l/P_l$, extracted from the in-loop sensor (PD1), were reduced at the level of 4.1×10^{-5} ($\Delta P_l \simeq 3$ nW) at 10^5 s. In this configuration, the clock Allan deviation, extracted from a shorter measurement (5 days) and given the confidence intervals, is comparable or very slightly improved at a level below 2×10^{-12} at 10^5 s.

5. Conclusions

We have reported the progress of a table-top CPT-based Cs atomic clock using a symmetric auto-balanced Ramsey (SABR) interrogation technique and a microfabricated cell, filled with Neon, with low permeation ASG windows. We demonstrated that ASG reduces significantly Ne permeation through the cell glass in comparison with standard borosilicate glass (BSG). This solution allows to mitigate the impact of the cell atmosphere evolution to the clock mid- and long-term stability. Since light-shift effects remained the main contribution to the clock stability for $\tau > 10^4$ s, we implemented active stabilization of the setup box temperature, microwave power and laser power. The addition of these servos contributed to yield a clock Allan deviation of 1.4×10^{-12} at 10^5 s. These results at 1 day, competitive with those of best microwave microcell-based atomic clocks [4, 14, 21], are more than 10 times better than obtained previously with this clock demonstrator [20]. In the future, the implementation of the pulsed SABR sequence without the use of an external AOM will be investigated. Several approaches might be explored for this purpose [29–31]. This might pave the way to the advent of new-generation fully-integrated pulsed CPT atomic clocks with enhanced stability.

Funding. C. Carlé's PhD thesis is co-funded by CNES (Centre National d'Etudes Spatiales) and AID (Agence Innovation Défense). This work was supported in part by DGA (Direction Générale de l'Armement), in part by Région de Franche-Comté, and in part by Agence Nationale de la Recherche (ANR) in the frame of the LabeX FIRST-TF (Grant No. ANR 10-LABX-0048), EquipX Oscillator-IMP (Grant No. ANR 11-EQPX-0033) and ASTRID PULSACION (Grant No. ANR-19-ASTR-0013-01) projects. This work was also partially supported by the French RENATECH network and its FEMTO-ST technological facility.

Disclosures. The authors declare no conflicts of interest.

Data availability. Data underlying the results presented in this paper are not publicly available at this time but may be obtained from the authors upon reasonable request.

References

1. S. Knappe, V. Shah, P.D.D. Schwindt, L. Hollberg, L.-A. Liew and J. Moreland, "A microfabricated atomic clock," Appl. Phys. Lett. **85**, 9, 1460–1462 (2004).
2. S. Knappe, "MEMS atomic clocks," in Compr. Microsystems, Y. B. Gianchandani, O. Tabata and H. Zappe, ed., (Elsevier, 2008), pp 571–612.
3. J. Kitching, "Chip-scale atomic devices," Appl. Phys. Rev. **5**, 031302 (2018).
4. H. Zhang, H. Hans, N. Tharayil, A. Shirane, M. Suzuki, K. Harasaka, K. Adachi, S. Goka, S. Yanagimachi, K. Okada, "ULPAC: A miniaturized ultra-low-power atomic clock," IEEE Journ. Solid State Circuits **54**, 11, 3135–3148 (2019).
5. R. Lutwak, A. Rashed, M. Varghese, G. Tepolt, J. LeBlanc, M. J. Mescher, D. K. Serkland, K. M. Geib, G. M. Peake, S. Römisch "The Chip-Scale Atomic Clock-Prototype Evaluation," Proc. 39th Annu. Precise Time Time Interval (PTTI) Meet., (The Institute of Navigation, 2007), pp. 269–290.
6. R. Lutwak, A. Rashed, M. Varghese, G. Tepolt, J. LeBlanc, M. J. Mescher, D. K. Serkland, G. M. Peake, "The Miniature Atomic Clock - Pre-Production Results," Proc. IEEE Int. Freq. Control. Symp. - Eur. Freq. Time Forum Jt. Meet., (IEEE, 2007), pp. 1237–1333.
7. J. Vanier, "Atomic clocks based on coherent population trapping: a review," Appl. Phys. B **81**, 4, 421–442 (2005).
8. M. Zhu and L. S. Cutler, "Theoretical and experimental study of light shift in a CPT-based Rb vapor cell frequency standard," Proc. 32nd Annu. Precise Time Time Interval (PTTI) Meet., (The Institute of Navigation, 2000), pp. 311-323.
9. V. Shah, V. Gerginov, P. D. D. Schwindt, S. Knappe, L. Hollberg and John Kitching, "Continuous light-shift correction in modulated coherent population trapping clocks," Appl. Phys. Lett. **89**, 151124 (2006).
10. B. H. McGuyer, Y.-Y. and W. Happer, "Simple method of light-shift suppression in optical pumping systems," Appl. Phys. Lett. **94**, 251110 (2009).
11. Y. Zhang, W. Yang, S. Zhang and J. Zhao, "Rubidium chip-scale atomic clock with improved long-term stability through light intensity optimization and compensation for laser frequency detunings," J. Opt. Soc. Am. B **33**, 8, 1756–1763 (2016).
12. D. Miletic, C. Affolderbach, M. Hasegawa, R. Boudot, C. Gorecki and G. Mileti, "AC Stark-shift in CPT-based Cs miniature atomic clocks," Appl. Phys. B **109**, 8, 89-97 (2012).
13. R. Vicarini, M. Abdel Hafiz, V. Maurice, N. Passilly, E. Kroemer, L. Ribetto, V. Gaff, C. Gorecki, S. Galliou and R. Boudot, "Mitigation of temperature-induced light-shift effects in miniaturized atomic clocks," IEEE Trans. Ultrason. Ferroelec. Freq. Contr. **66**, 12, 1962–1967 (2019).
14. S. Yanagimachi, S. Harasaka, R. Suzuki, M. Suzuki and S. Goka, "Reducing frequency drift caused by light shift in coherent population trapping-based low-power atomic clocks," Appl. Phys. Lett. **116**, 104102 (2020).
15. V. Yudin, M. Yu. Basalaev, A. V. Taichenachev, J. W. Pollock, Z. L. Newman, M. Shuker, A. Hansen, M. T. Hummon, R. Boudot, E. A. Donley and J. Kitching, "General methods for suppressing the light-shift in atomic clocks using power modulation," Phys. Rev. Appl. **14**, 024001 (2020).
16. M. Abdel Hafiz, R. Vicarini, N. Passilly, C. E. Calosso, V. Maurice, J. Pollock, A. Taichenachev, V. I .Yudin, J. Kitching and R. Boudot, "Protocol for light-shift compensation in a continuous-wave microcell atomic clock," Phys. Rev. Appl. **14**, 034015 (2020).
17. S. Micalizio, C. E. Calosso, A. Godone and F. Levi, "Metrological characterization of the pulsed Rb clock with optical detection," Metrologia **49**, 425-436 (2012).
18. M. Abdel Hafiz, G. Coget, M. Petersen, C. E. Calosso, S. Guérandel, E. de Clercq and R. Boudot, "Symmetric autobalanced Ramsey interrogation for high-performance coherent population-trapping vapor-cell atomic clock," Appl. Phys. Lett. **112**, 244102 (2018).
19. C. Carlé, M. Petersen, N. Passilly, M. Abdel Hafiz, E. de Clercq and R. Boudot, "Exploring the use of Ramsey-CPT spectroscopy for a microcell-based atomic clock," IEEE Trans. Ultrason. Ferroelec. Freq. Contr. **68**, 10, 3249–3256 (2021).

20. M. Abdel Hafiz, C. Carlé, N. Passilly, J.-M. Danet, C. E. Calosso and Rodolphe Boudot, "Light-shift mitigation in a microcell-based atomic clock with symmetric auto-balanced Ramsey spectroscopy," Appl. Phys. Lett. **120**, 064101 (2022).
21. E. Batori, C. Affolderbach, M. Pellaton, F. Gruet, M. Violetti, Y. Su, A. K. Skrivervik and G. Mileti, "μPOP clock: A microcell atomic clock based on a double-resonance Ramsey scheme," Phys. Rev. Appl. **18**, 054039 (2022).
22. O. Kozlova and S. Guérandel and E. de Clercq, "Temperature and pressure shift of the Cs clock transition in the presence of buffer gases: Ne, N_2, Ar," Phys. Rev. A **83**, 062714 (2011).
23. S. Abdullah, C. Affolderbach, F. Gruet and G. Mileti, "Aging studies on micro-fabricated alkali buffer-gas cells for miniature atomic clocks," Appl. Phys. Lett. **106**, 163505 (2015).
24. A. T. Dellis and V. Shah and E. A. Donley and S. Knappe and J. Kitching, "Low helium permeation cells for atomic microsystems technology," Opt. Lett. **41**, 12, 2775–2778 (2016).
25. J. P. McGilligan and K. R. Moore and A. Dellis and G. D. Martinez and E. de Clercq and P. F. Griffin and A. S. Arnold and E. Riis and R. Boudot and J. Kitching, "Laser cooling in a chip-scale platform," Appl. Phys. Lett. **117**, 054001 (2020).
26. R. Vicarini, V. Maurice, M. Abdel Hafiz, J. Rutkowski, C. Gorecki, N. Passilly, L. Ribetto, V. Gaff, V. Volant, S. Galliou and R. Boudot, "Demonstration of the mass-producible feature of a Cs vapor microcell technology for miniature atomic clocks," Sens. Actuat. A: Phys. **280**, 99-106 (2018).
27. E. Kroemer, J. Rutkowski, V. Maurice, R. Vicarini, M. Abdel Hafiz, C. Gorecki, and R. Boudot, "Characterization of commercially available vertical-cavity surface-emitting lasers tuned on Cs D_1 line at 894.6 nm for miniature atomic clocks," Appl. Opt. **55**, 31, 8839–8847 (2016).
28. J. Shelby, "Helium, deuterium, and neon migration in a common borosilicate glass," J. Appl. Phys. **45**, 5, 2146–2149 (1974).
29. T. Ide, S. Goka and Y. Yano, "CPT pulse excitation method based on VCSEL current modulation for miniature atomic clocks," Proc. IEEE Int. Freq. Control. Symp. - Eur. Freq. Time Forum Jt. Meet., (IEEE, 2015), pp. 269–290.
30. J. Yang, Y. Tian, B. Tan, P. Yun and S. Gu, "Exploring Ramsey-coherent population trapping atomic clock realized with pulsed microwave modulator laser," J. Appl. Phys. **115**, 093109 (2014).
31. M. Jafati, I. J. Guo and M. Rais-Zadeh, "An ultra-fast optical shutter exploiting total light absorption in a phase change material," Proc. SPIE **10000**, 101000I (2017).